第 43 卷 第 18 期/2023 年 9 月/光学学报 封底文章·特邀研究论文

光学学报

T字头石英音叉的设计及其气体传感性能

房超，乔顺达，何应，申作春，马欲飞*

哈尔滨工业大学航天学院可调谐激光技术国家级重点实验室，黑龙江 哈尔滨 150001

摘要 首先，利用有限元分析方法，仿真模拟了石英音叉的应力和表面电荷分布，设计并加工了一种T字头石英音叉。经过实测，此T字头石英音叉的共振频率为8930.93 Hz，Q值为11164，叉指间距为1.73 mm，与目前广泛应用的商用石英音叉相比，T字头石英音叉的共振频率降低了73%，品质因数提高了22%。然后，通过测量水汽对其传感性能进行验证，发现相比于商用石英音叉，基于T字头石英音叉的石英增强光声光谱（QEPAS）系统信噪比提升了60.65%。最后，给出了石英音叉下一步优化的方向。

关键词 遥感；石英音叉；石英增强光声光谱；有限元分析；品质因数；信噪比

中图分类号 O436 **文献标志码** A **DOI：** 10.3788/AOS231163

1 引 言

近年来，大气中有害气体逐渐成为人们关注的重要问题，它不仅会危害人体健康，还会对环境造成严重污染，从而引发一系列生态问题[1-2]。同时，工业生产及医疗诊断等领域也对痕量气体的监测提出了更高的要求。气体传感技术可以对痕量气体浓度进行高灵敏度监测，获知气体的组分、浓度及其分布变化[3-7]。

常见的气体传感技术可分为非光谱式和光谱式两类[8-10]，其中非光谱式传感技术具有响应时间长、无法实时监测等局限性，而光谱式传感技术基于气体分子的“指纹”吸收特性，具有检测灵敏度高、选择性好、可以对气体浓度进行实时监测等优点[11-18]。在传统的光声光谱传感技术中，使用麦克风作为探测元件，检测气体吸收激光产生的声波信号，进而计算出气体浓度[19]。但是麦克风响应频带较宽，很容易受到环境中其他声波噪声的干扰，导致测量结果不稳定。为了解决这一问题，2002年美国莱斯大学Frank Tittel教授课题组提出了石英增强光声光谱技术（QEPAS）[20]，使用石英音叉（QTF）代替麦克风进行声波信号探测，石英音叉具有响应带宽窄、抗噪声能力强、品质因数高等优点[21-28]。石英音叉是QEPAS技术中的核心元件，但目前该技术领域中广泛使用的、共振频率为32.768 kHz的商用石英音叉还存在一定的局限性[29-36]，如：共振频率过高，无法对分子弛豫率低的气体进行检测；能量积累时间短，导致系统对声波信号的收集能力弱；石英音叉叉指间距小，不利于激光束从中间穿过，导致调节难度大。意大利Spagnolo课题组[37-39]近年来也开展了石英音叉优化设计研究。

本文针对目前常见QEPAS技术中石英音叉性能存在不足的现状，从有限元分析的角度出发，建立了仿真模型，获得了一种性能优异的T字头石英音叉，并通过实验对其性能进行分析。在理论设计和实验验证环节，将所设计的T字头石英音叉与常见的共振频率为32.768 kHz的商用石英音叉进行了对照。最后，提出了关于石英音叉优化设计的改进措施。

2 基本原理及仿真研究

石英音叉的共振频率由其组成材料的特性和设计的尺寸大小来决定[40-41]，表达式为

$$f_n=\frac{\pi d}{8\sqrt{12}\,L^2}\sqrt{\frac{E}{\rho}}\,n^2\,,\tag{1}$$

式中：ρ为石英的密度；E为杨氏模量；d为石英音叉的叉指厚度；L为石英音叉的叉指长度；n为模式数。品质因数Q与组成材料的材质有关，是系统能量损失的量度，忽略一些损失，其表达式[42]可简化为

$$Q\propto\frac{8}{3}\frac{\rho w\sqrt{f_0}}{\sqrt{\pi\rho_0\mu}}\propto\frac{\omega d}{L},\tag{2}$$

式中：ω为石英音叉的叉指宽度。从式(2)看到，可以通过提高石英音叉的叉指宽度、降低叉指长度、增大叉指厚度的方式来提高其整体品质因数。共振频率f_0和

收稿日期：2023-06-20；**修回日期**：2023-07-10；**录用日期**：2023-08-02；**网络首发日期**：2023-08-15

基金项目：国家自然科学基金优秀青年科学基金（62022032）、国家自然科学基金（62275065，61875047，61505041）、安徽大学光电信息获取与控制教育部重点实验室（OEIAM202202）、中央高校基本科研业务费专项

通信作者：*mayufei@hit.edu.cn

品质因数共同决定了能量积累时间[21]，表达式为

$$t=\frac{Q}{f_0}。 \tag{3}$$

在 COMSOL 仿真软件中，选取固体力学(solid)模块和静电(es)模块，根据表 1 的石英音叉尺寸建立三维仿真模型，将材料设置为 Quartz LH(1949 IRE)，选中建好的石英音叉模型侧面并将固体力学模块中的边界载荷设定为 1 Pa，静电模块中的接地选项设定为除石英音叉底座的所有域，选中多物理场的压电效应(pze1)，通过添加特征频域研究得到不同频域的振型图。

通过研究得到共振频率分别为 32767.76 Hz、8999 Hz 的商用石英音叉和 T 字头石英音叉的仿真模型。商用石英音叉的表面电荷密度和应力分布如图 1(a)、(b)所示，最大应力值为 1.65×10^{7} N/m^2，平均表面电荷密度为 3.1412×10^{-6} C/m^2。T 字头石英音叉的表面电荷密度和应力分布如图 2(a)、(b)所示，其最大应力值为 9.2×10^{7} N/m^2，平均表面电荷密度为 6.7355×10^{-6} C/m^2。相较于商用石英音叉，T 字头石英音叉的最大应力值提高了 4.58 倍，平均表面电荷密度提高了 1.14 倍，这主要得益于 T 字头石英音叉的尖端采用了 2.4 mm×2 mm 的长方形设计，使得整个石英音叉的重心升高，增大了在振动过程中的受力力矩，使得石英音叉在共振过程中的振动幅度变大，石英音叉根部所受应力得到了增强，从而使得信号的收集效率更高。此外，通过式(1)、(2)中共振频率和品质因数与各个参量之间的关系，最终得到叉指长度为 9.4 mm、叉指宽度为 1.2 mm、叉指厚度为 0.25 mm、叉指间距为 1.73 mm 的最佳尺寸设计。该设计既降低了共振频率、提高了品质因数、增强了石英音叉对声波的收集能力，又扩大了叉指间距，有利于光束的准直传输，并降低了系统光学噪声。

表 1　两种石英音叉的尺寸对比

Table 1　Size comparison of two QTFs　unit: mm

QTF type	Length	Width	Thickness	Space
Commercial QTF	3.9	0.6	0.36	0.3
T-head QTF	9.4	1.2	0.25	1.73

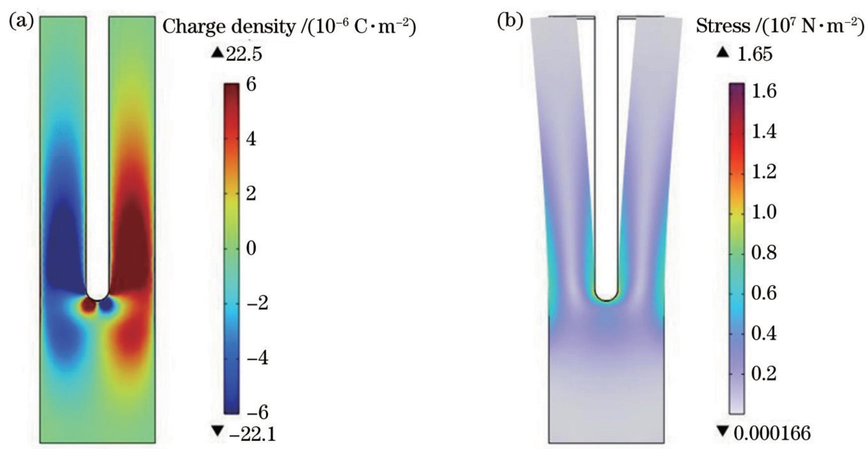

图 1　商用小型石英音叉的仿真结果图。(a)表面电荷密度分布；(b)应力分布

Fig. 1　Simulation results of commercial QTF. (a) Surface charge density distribution; (b) stress distribution

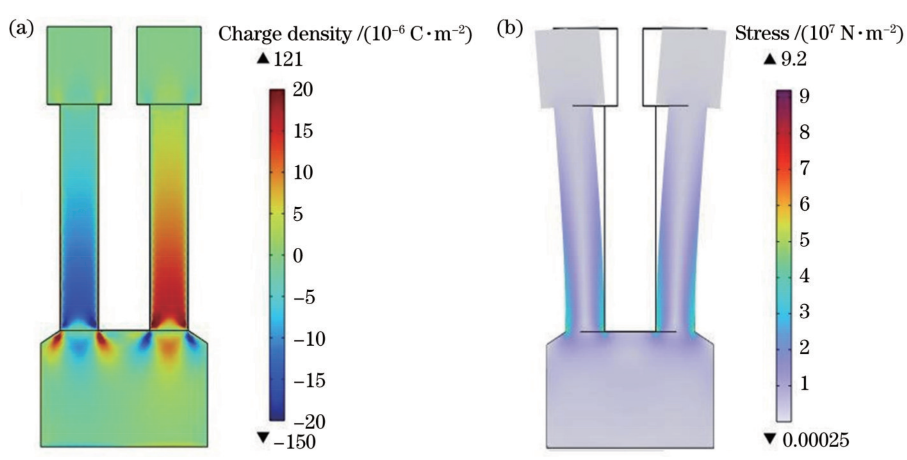

图 2　T 字头石英音叉的仿真结果。(a)表面电荷密度分布；(b)应力分布

Fig. 2　Simulation results of T-head QTF. (a) Surface charge density distribution; (b) stress distribution

3 实验装置

在实验验证环节，以大气中的水汽为测量对象。QEPAS 水汽探测系统如图 3(a)所示，选择位于 1368.6 cm^{-1} 的水汽吸收线，锁相放大器输出的正弦信号与信号发生器产生的锯齿波相互叠加，用于调节激光控制器，激光器温度设置为 35 ℃。调节位移台，使得激光光束入射到石英音叉的叉指间隙，此处的水汽分子吸收激光能量，产生光声信号，基于石英音叉的压电效应，此声波信号被转换为电信号，将其传输到锁相放大器，解调得到二次谐波信号(2*f*)。在相同条件下，利用该系统测试了图 3(b)所示的两种石英音叉，其中一种是商用石英音叉，另一种是所设计的 T 字头石英音叉。

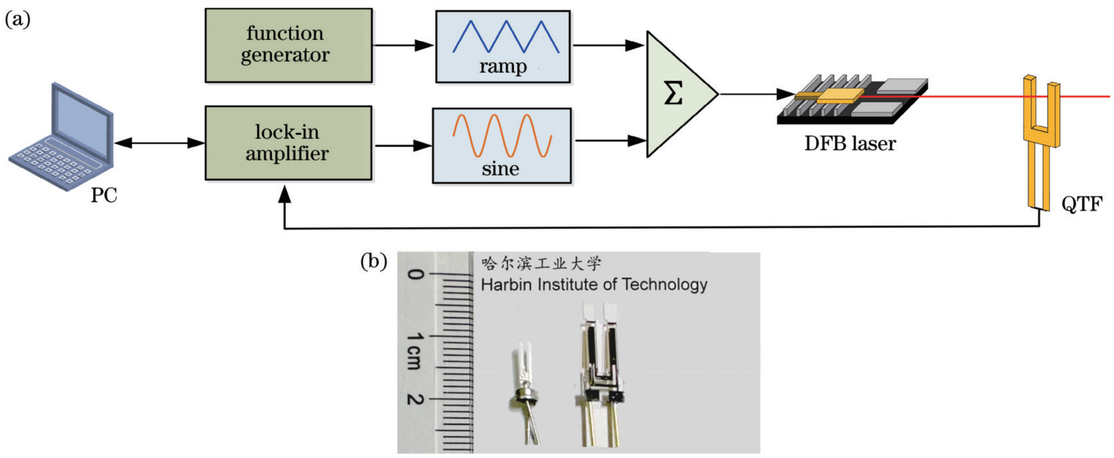

图 3 QEPAS 传感系统。(a) QEPAS 水汽探测系统；(b) 两种石英音叉实物图

Fig. 3 QEPAS sensing system. (a) H_2O-QEPAS detection system; (b) actual illustration of two QTFs

4 分析与讨论

采用光学激励的方法，首先分别对商用石英音叉和 T 字头石英音叉的性能进行测试。商用石英音叉的共振频率曲线如图 4(a)所示，其共振频率 f_0 为 32767.76 Hz，品质因数为 9128；T 字头石英音叉的共振频率如图 4(b)所示，其 f_0 为 8930.93 Hz，品质因数为 11164。与商用石英音叉相对比，T 字头石英音叉的共振频率约下降了 73%，品质因数提高了 22%。根据式(2)，其能量积累时间提高了 3.50 倍。

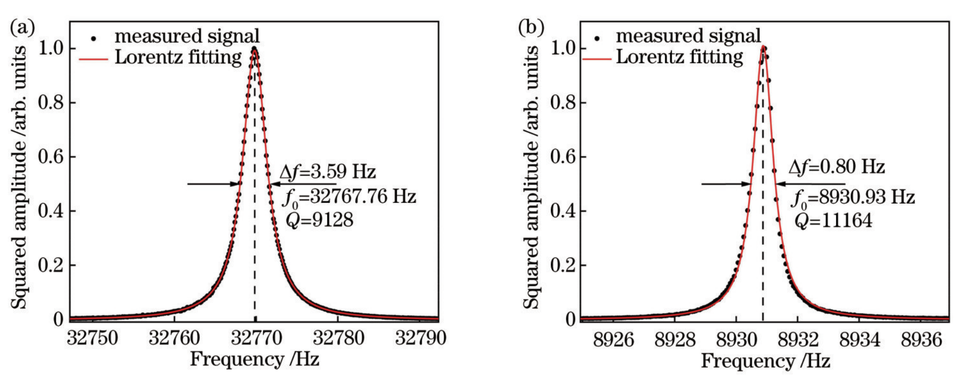

图 4 两种石英音叉的频率响应曲线。(a) 商用石英音叉；(b) T 字头石英音叉

Fig. 4 Frequency response curves of two QTFs. (a) Commercial QTF; (b) T-head QTF

实验测得的商用石英音叉和 T 字头石英音叉的参数如表 2 所示，可以看出，虽然 T 字头石英音叉的等效阻值 *R* 很高，而石英音叉的内阻升高会导致音叉电荷产生效率降低，进而影响气体探测性能，但共振频率 f_0 明显降低，品质因数 *Q* 也有小幅度提高。这些性能的提高将有助于 T 字头石英音叉应用到气体传感领域，使得传感系统的整体探测性能得到增强。低共振频率的 T 字头石英音叉还可以检测分子弛豫率低的气体，使得检测气体的范围更广。

表 2 不同石英音叉参数对比

Table 2 Parameter comparison of different QTFs

QTF type	f_0 /Hz	R /kΩ	Q
Commercial QTF	32767.76	122.1	9128
T-head QTF	8930.93	362.8	11164

对上述两种石英音叉的传感性能进行测试。为了优化水汽探测系统，对激光波长调制深度进行优化，以提高信号幅值。扫描的激光调制深度结果如图 5(a)、 (b)所示,可以看到,基于商用石英音叉的QEPAS传感系统的最佳调制电流为16.55 mA,基于T字头石英音叉的QEPAS传感系统的最佳调制电流为6.16 mA。在不同的调制频率下,激光器对应的电流调制系数不同,频率越高,调制系数越小,从而导致QEPAS系统的最佳调制电流不同。由于QEPAS系统中采用的T字头石英音叉和普通石英音叉需要不同的调制频率,因此系统优化得到的最佳调制电流也不一致。

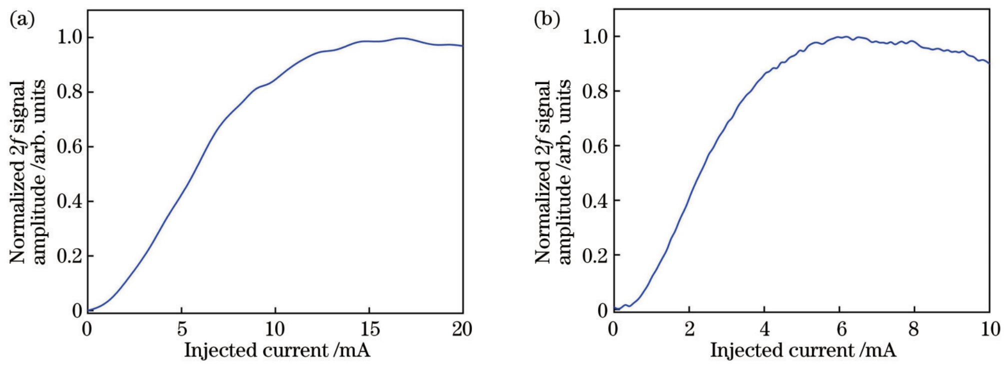

图5 QEPAS传感系统的调制深度曲线。(a) 商用石英音叉;(b) T字头石英音叉

Fig. 5 Modulation depth curves of QEPAS sensing system. (a) Commercial QTF; (b) T-head QTF

激光束通过石英音叉的叉指间隙就可以产生光声信号,由于声源位置会影响力矩的大小,而力矩的大小决定了光声信号的强弱,因此QEPAS系统的信号强度与激光入射位置有关,需要寻找一个最佳的激光源入射位置,使得信号幅值达到最大。商用石英音叉和T字头石英音叉的位置优化结果分别如图6(a)、(b)所示,其中ΔL表示激光入射点到顶部的垂直距离,1.66%为H_2O分子浓度。商用石英音叉的最佳激光入射位置在距离顶端0.7 mm处,T字头石英音叉的最佳激光入射位置在距离顶端1.6 mm处。

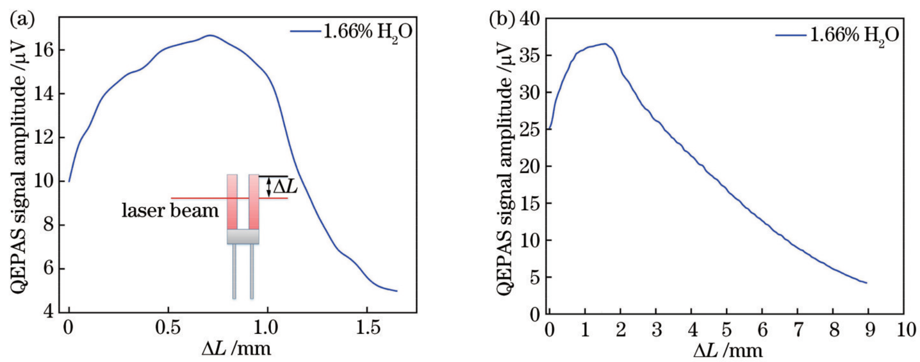

图6 石英音叉位置优化结果。(a) 商用小型石英音叉;(b) T字头石英音叉

Fig. 6 QTF′s position optimization results. (a) Commercial QTF; (b) T-head QTF

采用上述确定的最佳调制电流和最佳激光入射位置,分别测量了基于商用石英音叉和T字头石英音叉的水汽2*f*信号,测试结果如图7所示,通过计算2*f*信号侧翼部分可以得到系统的噪声。从图7可以看到:采用商用石英音叉测得的水汽2*f*信号幅值为16.44 μV,噪声为58.86 nV,信噪比为279.31;采用T字头石英音叉测得的水汽2*f*信号幅值为25.37 μV,噪声为56.54 nV,信噪比为448.71。相比于商用石英音叉,采用T字头石英音叉探测得到的信号幅值提高了54.32%,信噪比提升了60.65%。这些改善主要得益于T字头石英音叉的能量积累时间较长,系统对声波信号的收集能力得到提高,同时叉指间距的增大避免了探测环境中其他噪声信号的干扰。

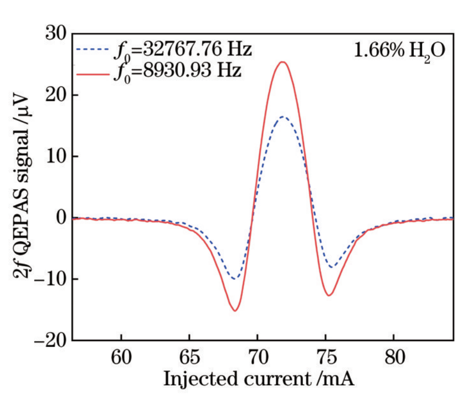

图7 采用不同石英音叉的QEPAS系统测量的2*f*信号

Fig. 7 2*f* signal detected by QEPAS system with different QTFs

5 结 论

通过有限元分析方法仿真出具有低共振频率、高Q值、大叉指间距的T字头石英音叉。经过实测，此T字头石英音叉的共振频率为8930.93 Hz、Q值为11164、叉指间距为1.73 mm，与目前广泛应用的商用石英音叉相比，T字头石英音叉的共振频率降低了73%，品质因数提高了22%。将此石英音叉应用到近红外QEPAS水汽探测系统中，进一步检测其传感性能。与商用石英音叉相比，基于T字头石英音叉的水汽QEPAS系统的信噪比提升了60.65%，证明了此石英音叉具有优越的传感性能。但此石英音叉的等效电阻值仍然过高，对整体探测性能存在影响，后续将进一步优化，降低等效电阻值，以进一步提升系统的传感性能。

参 考 文 献

[1] Kocache R. The measurement of oxygen on gas mixtures[J]. Journal of Physics E, 1986, 19(6): 401-412.

[2] Khalil M A K, Rasmussen R A. Carbon monoxide in the earth's atmosphere: increasing trend[J]. Science, 1984, 224(4644): 54-56.

[3] Zhang Z D, Peng T, Nie X Y, et al. Entangled photons enabled time-frequency-resolved coherent Raman spectroscopy and applications to electronic coherences at femtosecond scale[J]. Light: Science & Applications, 2022, 11: 274.

[4] Ma Y F, He Y, Tong Y, et al. Quartz-tuning-fork enhanced photothermal spectroscopy for ultra-high sensitive trace gas detection[J]. Optics Express, 2018, 26(24): 32103-32110.

[5] Yan M, Luo P L, Iwakuni K, et al. Mid-infrared dual-comb spectroscopy with electro-optic modulators[J]. Light: Science & Applications, 2017, 6(10): e17076.

[6] Hashimoto K, Nakamura T, Kageyama T, et al. Upconversion time-stretch infrared spectroscopy[J]. Light: Science & Applications, 2023, 12: 48.

[7] Liu Y H, Ma Y F. Advances in multipass cell for absorption spectroscopy-based trace gas sensing technology[J]. Chinese Optics Letters, 2023, 21(3): 033001.

[8] Mao Y H, Zhao D, Yan S, et al. A vacuum ultraviolet laser with a submicrometer spot for spatially resolved photoemission spectroscopy[J]. Light: Science & Applications, 2021, 10: 22.

[9] 马欲飞. 基于石英增强光声光谱的气体传感技术研究进展[J]. 物理学报, 2021, 70(16): 160702.
Ma Y F. Research progress of quartz-enhanced photoacoustic spectroscopy based gas sensing[J]. Acta Physica Sinica, 2021, 70(16): 160702.

[10] Wang Y F, Du H Y, Li Y Q, et al. Testing universality of Feynman-Tan relation in interacting Bose gases using high-order Bragg spectra[J]. Light: Science & Applications, 2023, 12: 50.

[11] Zhang C, Qiao S D, He Y, et al. Differential quartz-enhanced photoacoustic spectroscopy[J]. Applied Physics Letters, 2023, 122(24): 241103.

[12] Lin H N, Cheng J X. Computational coherent Raman scattering imaging: breaking physical barriers by fusion of advanced instrumentation and data science[J]. eLight, 2023, 3(1): 1-19.

[13] Ma Y F, Liang T T, Qiao S D, et al. Highly sensitive and fast hydrogen detection based on light-induced thermoelastic spectroscopy[J]. Ultrafast Science, 2023, 3: 0024.

[14] Yang W, Knorr F, Latka I, et al. Real-time molecular imaging of near-surface tissue using Raman spectroscopy[J]. Light: Science & Applications, 2022, 11: 90.

[15] He Y, Ma Y F, Tong Y, et al. Ultra-high sensitive light-induced thermoelastic spectroscopy sensor with a high Q-factor quartz tuning fork and a multipass cell[J]. Optics Letters, 2019, 44(8): 1904-1907.

[16] Le J M, Su Y D, Tian C S, et al. A novel scheme for ultrashort terahertz pulse generation over a gapless wide spectral range: Raman-resonance-enhanced four-wave mixing[J]. Light: Science & Applications, 2023, 12: 34.

[17] Qiao S D, Ma P Z, Tsepelin V, et al. Super tiny quartz-tuning-fork-based light-induced thermoelastic spectroscopy sensing[J]. Optics Letters, 2023, 48(2): 419-422.

[18] Chen G Y, Sun Y B, Shi P C, et al. Revealing unconventional host-guest complexation at nanostructured interface by surface-enhanced Raman spectroscopy[J]. Light: Science & Applications, 2021, 10: 85.

[19] Zhang C, Qiao S D, Ma Y F. Highly sensitive photoacoustic acetylene detection based on differential photoacoustic cell with retro-reflection-cavity[J]. Photoacoustics, 2023, 30: 100467.

[20] Kosterev A A, Bakhirkin Y A, Curl R F, et al. Quartz-enhanced photoacoustic spectroscopy[J]. Optics Letters, 2002, 27(21): 1902-1904.

[21] Li S Z, Dong L, Wu H P, et al. Ppb-level quartz-enhanced photoacoustic detection of carbon monoxide exploiting a surface grooved tuning fork[J]. Analytical Chemistry, 2019, 91(9): 5834-5840.

[22] Lin H Y, Zheng H D, Montano B A Z, et al. Ppb-level gas detection using on-beam quartz-enhanced photoacoustic spectroscopy based on a 28 kHz tuning fork[J]. Photoacoustics, 2022, 25: 100321.

[23] Ma Y F, Lewicki R, Razeghi M, et al. QEPAS based ppb-level detection of CO and N_2O using a high power CW DFB-QCL[J]. Optics Express, 2013, 21(1): 1008-1019.

[24] Zifarelli A, De Palo R, Patimisco P, et al. Multi-gas quartz-enhanced photoacoustic sensor for environmental monitoring exploiting a Vernier effect-based quantum cascade laser[J]. Photoacoustics, 2022, 28: 100401.

[25] Patimisco P, Sampaolo A, Zheng H D, et al. Quartz-enhanced photoacoustic spectrophones exploiting custom tuning forks: a review[J]. Advances in Physics X, 2017, 2(1): 169-187.

[26] Hu Y Q, Qiao S D, He Y, et al. Quartz-enhanced photoacoustic-photothermal spectroscopy for trace gas sensing [J]. Optics Express, 2021, 29(4): 5121-5127.

[27] Liu X N, Ma Y F. Sensitive carbon monoxide detection based on light-induced thermoelastic spectroscopy with a fiber-coupled multipass cell[J]. Chinese Optics Letters, 2022, 20(3): 031201.

[28] Ma Y F, Tong Y, He Y, et al. Research progress of quartz-enhanced photoacoustic spectroscopy[J]. Chinese Journal of Luminescence, 2017, 38(7): 839-848.

[29] Ma Y F. Recent advances in QEPAS and QEPTS based trace gas sensing: a review[J]. Frontiers in Physics, 2020, 8: 268.

[30] Patimisco P, Sampaolo A, Dong L, et al. Recent advances in quartz enhanced photoacoustic sensing[J]. Applied Physics Reviews, 2018, 5(1): 011106.

[31] Wu H P, Dong L, Yin X K, et al. Atmospheric CH_4 measurement near a landfill using an ICL-based QEPAS sensor with V-T relaxation self-calibration[J]. Sensors and Actuators B, 2019, 297: 126753.

[32] Qiao S D, He Y, Ma Y F. Trace gas sensing based on single-quartz-enhanced photoacoustic-photothermal dual spectroscopy [J]. Optics Letters, 2021, 46(10): 2449-2452.

[33] Wu H P, Dong L, Zheng H D, et al. Beat frequency quartz-enhanced photoacoustic spectroscopy for fast and calibration-free continuous trace-gas monitoring[J]. Nature Communications, 2017, 8: 15331.

[34] 胡立兵, 刘锟, 王贵师, 等. 基于2.33 μm可调谐激光的石英音叉增强型光声光谱测量CO研究[J]. 激光与光电子学进展,

2015, 52(5): 053002.
Hu L B, Liu K, Wang G S, et al. Research on detecting CO with quartz enhanced photoacoustic spectroscopy based on 2.33 μm distributed feed back laser[J]. Laser & Optoelectronics Progress, 2015, 52(5): 053002.

[35] 张蕾蕾, 刘家祥, 朱之贞, 等. 基于石英增强光声光谱的 H_2S 痕量气体检测研究[J]. 激光与光电子学进展, 2019, 56(21): 213001.
Zhang L L, Liu J X, Zhu Z Z, et al. Detection of trace sulfur dioxide gas using quartz-enhanced photoacoustic spectroscopy[J]. Laser & Optoelectronics Progress, 2019, 56(21): 213001.

[36] 张明辉, 胡立恩, 姚丹, 等. 石英音叉增强光声光谱甲烷检测系统[J]. 光学学报, 2020, 40(24): 2430001.
Zhang M H, Hu L E, Yao D, et al. Quartz tuning fork enhanced photoacoustic spectroscopic methane detection system [J]. Acta Optica Sinica, 2020, 40(24): 2430001.

[37] Spagnolo V, Kosterev A A, Dong L, et al. NO trace gas sensor based on quartz-enhanced photoacoustic spectroscopy and external cavity quantum cascade laser[J]. Applied Physics B, 2010, 100(1): 125-130.

[38] Patimisco P, Sampaolo A, Giglio M, et al. Tuning forks with optimized geometries for quartz-enhanced photoacoustic spectroscopy[J]. Optics Express, 2019, 27(2): 1401-1415.

[39] Sgobba F, Sampaolo A, Patimisco P, et al. Compact and portable quartz-enhanced photoacoustic spectroscopy sensor for carbon monoxide environmental monitoring in urban areas[J]. Photoacoustics, 2022, 25: 100318.

[40] Patimisco P, Sampaolo A, Dong L, et al. Analysis of the electro-elastic properties of custom quartz tuning forks for optoacoustic gas sensing[J]. Sensors and Actuators B, 2016, 227: 539-546.

[41] Patimisco P, Borri S, Sampaolo A, et al. A quartz enhanced photo-acoustic gas sensor based on a custom tuning fork and a terahertz quantum cascade laser[J]. Analyst, 2014, 139(9): 2079-2087.

[42] Hosaka H, Itao K, Kuroda S. Damping characteristics of beam-shaped micro-oscillators[J]. Sensors and Actuators A, 1995, 49 (1/2): 87-95.

Design and Sensing Performance of T-Shaped Quartz Tuning Forks

Fang Chao, Qiao Shunda, He Ying, Shen Zuochun, Ma Yufei*
National Key Laboratory of Science and Technology on Tunable Laser, Harbin Institute of Technology, Harbin 150001, *Heilongjiang, China*

Abstract

Objective In recent years, harmful gases in the atmosphere have gradually become an important issue of concern for people. Gas sensing technology can perform highly sensitive monitoring of trace gas concentrations, obtaining information on the composition, knowing the concentration changes of gases, and understanding the distribution changes of gases. Quartz-enhanced photoacoustic spectroscopy (QEPAS) technology based on quartz tuning fork detection has the advantages of simple structure, low cost, and strong anti-noise ability, which is a hot spot in the field of gas sensing. In common QEPAS technology, commercial quartz tuning forks are generally used with a resonance frequency of 32.768 kHz, but the performance of QEPAS systems is limited due to high resonance frequency, short energy accumulation time, and small interfinger spacing.

Methods In this paper, the finite element analysis method is used to simulate the stress and charge distribution of quartz tuning forks. A T-shaped quartz tuning fork is designed, and the resonance frequency of the T-shaped quartz tuning fork is 8930.93 Hz, with a Q value of 11164 and a cross interfinger spacing of 1.73 mm. In the experimental verification phase, by using water vapor in the atmosphere as the measurement object, the QEPAS water vapor detection system is built. Under the same conditions, we test two types of quartz tuning forks. One is a commercial quartz tuning fork, and the other is a T-shaped quartz tuning fork. A comparison of experimental results between these two quartz tuning forks is performed to verify their detection performance.

Results and Discussions The T-shaped quartz tuning fork has a length of 9.4 mm, a width of 1.2 mm, and a thickness of 0.25 mm (Table 1). By using the optical excitation method, firstly, the performance of commercial quartz tuning forks and T-shaped quartz tuning forks is tested separately, so as to obtain the resonance frequency curves of two types of quartz tuning forks. The resonance frequency f_0 of a commercial quartz tuning fork is 32767.76 Hz, and the quality factor is 9128. f_0 of the T-shaped quartz tuning fork is 8930.93 Hz, and the quality factor is 11164. The resonance frequency of the T-shaped quartz tuning fork is reduced by 73%, and the quality factor is improved by 22% compared with the widely used commercial quartz tuning fork (Fig. 4). The signal level of the QEPAS system is related to the laser incidence position. The optimal laser incidence position for commercial quartz tuning forks is 0.7 mm from the top, and the optimal laser incidence position for T-shaped quartz tuning forks is 1.6 mm from the top (Fig. 6). The amplitude of the $2f$ signal using a commercial quartz tuning fork is 16.44 μV, and the noise level and the signal-to-noise ratio are 58.86 nV and 279.31, respectively. The amplitude of the $2f$ signal measured using a T-shaped quartz tuning fork is 25.37 μV, and the noise level and the signal-to-noise ratio are 56.54 nV and 448.71, respectively. Compared with commercial quartz tuning forks, the signal amplitude detected by T-shaped quartz tuning forks has increased by 54.32%, and the signal-to-noise ratio has increased by 60.65% (Fig. 7).

Conclusions The commercial quartz tuning forks widely used in QEPAS technology currently have certain limitations. For example, the high resonance frequency makes the system unable to detect gases with low molecular relaxation rates, short energy accumulation time leads to weak collection ability of acoustic signals, and small interdigital spacing is not conducive to coupling transmission of laser beams and reducing system noise. We use finite element analysis to simulate a T-shaped quartz tuning fork with low resonance frequency, high Q value, and large interdigital gap. After actual measurement, the resonance frequency of this T-shaped quartz tuning fork is 8930.93 Hz with a Q value of 11164 and interdigital spacing of 1.73 mm. Compared with the widely used commercial quartz tuning fork, the resonance frequency of the T-shaped quartz tuning fork is reduced by 73%, and the quality factor is increased by 22%. Finally, this quartz tuning fork is applied to the near-infrared QEPAS water vapor detection system to further verify its sensing performance. Compared with commercial quartz tuning forks, the signal-to-noise ratio of the water vapor QEPAS system based on the T-shaped quartz tuning fork has increased by 60.65%, proving the superiority of the sensing performance of this quartz tuning fork. However, the equivalent resistance value of this quartz tuning fork is still too high, which has an impact on the overall detection performance. Further optimization will be carried out to reduce the equivalent resistance value and further improve the sensing performance of the system.

Key words remote sensing; quartz tuning fork; quartz-enhanced photoacoustic spectroscopy (QEPAS); finite element analysis; quality factor; signal-to-noise ratio (SNR)